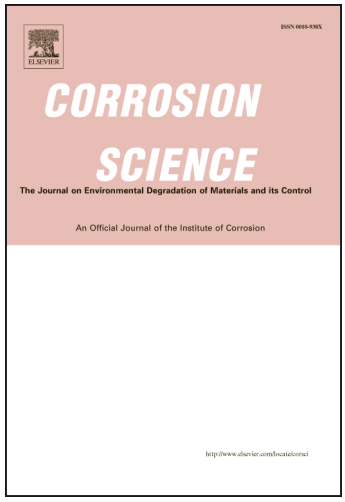

Corrosion of magnesium alloy AZ31: The influence of bicarbonate, sulphate, hydrogen phosphate and dihydrogen phosphate ions in saline solution

Rong-Chang Zeng, Yan Hu, Shao-Kang Guan, Hong-Zhi Cui, En-Hou Han

PII: S0010-938X(14)00233-9
DOI: http://dx.doi.org/10.1016/j.corsci.2014.05.006
Reference: CS 5856

To appear in: *Corrosion Science*

Received Date: 29 August 2013
Accepted Date: 6 May 2014

Please cite this article as: R-C. Zeng, Y. Hu, S-K. Guan, H-Z. Cui, E-H. Han, Corrosion of magnesium alloy AZ31: The influence of bicarbonate, sulphate, hydrogen phosphate and dihydrogen phosphate ions in saline solution, *Corrosion Science* (2014), doi: http://dx.doi.org/10.1016/j.corsci.2014.05.006

Corrosion of magnesium alloy AZ31: The influence of bicarbonate, sulphate, hydrogen phosphate and dihydrogen phosphate ions in saline solution

Rong-Chang Zeng [a, b,*], Yan Hu [a], Shao-Kang Guan [c], Hong-Zhi Cui [a], En-Hou Han [b]

[a] College of Materials Science and Engineering, Shandong University of Science and Technology, Qingdao 266590, China

[b] State Key Laboratory for Corrosion and Protection, Institute of Metals Research, Chinese Academy of Sciences, Shenyang 110016, China

[c] School of Materials Science and Engineering, Zhengzhou University, Zhengzhou 450002, China

Abstract:

The effects of anions in saline solutions on the corrosion behaviour of magnesium alloy AZ31 were investigated using hydrogen evolution, pH and potentiodynamic measurements. The results demonstrated that adding bicarbonate and sulphate ions to saline solution accelerated the corrosion, whereas hydrogen phosphate and dihydrogen phosphate retarded the corrosion and decreased the open-circuit potentials. A model involving the magnesium hydroxide and magnesium carbonate film formation mechanism was proposed. The change in the solution pH over time did not reflect the corrosion rates of the magnesium alloys due to the influence of anions.

Keywords: A: Magnesium; A: Alloy; B: Polarisation; B: SEM

1. Introduction

In the last decade, magnesium and its alloys have been identified as potential biodegradable

*Corresponding author. Tel. +86-532-80681226; fax: +86-532-86057920.
E-mail address: rczeng@gmail.com; rczeng@foxmail.com (R.C. Zeng)

biomaterials because they are highly biocompatible and have mechanical properties similar to human bones [1-3]. Attempts have been made to manipulate commercial magnesium alloys, such as AZ91D, LAE442, AE21, AZ31 and WE43, as bio-absorbable stents and orthopaedic devices [4-6]. In vivo tests reveal that the magnesium alloys degrade so quickly that they cannot support blood vessel walls or fractured bones during the healing process in blood plasma or human body fluids [4]. Therefore, tailoring the degradation rate of magnesium alloys used as degradable biomaterials is critical.

Usually, the in vitro lifetime of implanted devices must be predicted. The corrosion behaviours of magnesium alloys are predominately affected by their environments [7-16], chemical compositions (i.e., alloying elements [6, 8, 16-17] and impurities [18-21]), microstructure (grain size [22-24] and intermetallics [25]) and post-processing (i.e., extrusion processes [24, 26] and surface modification [27-31]) as well as corrosion products [22]. To date, numerous in vitro and in vivo corrosion studies have assessed magnesium alloys in simulated body fluids (SBFs) [11, 32], various animals [4, 6, 13, 33] and even patients [5]. Inorganic salts, amino acids and proteins significantly impact the in vitro degradation behaviour of pure magnesium alloys, such as AZ31, AZ91 and Mg-Ca alloys [8, 9, 12, 34-35]. For example, the mutual influences of Cl^-, HCO_3^-, HPO_4^{2-} and SO_4^{2-} on the corrosion behaviour of commercial die-cast AZ91 alloys in the physiological environment have been investigated [11, 36]. However, the influences of each individual anion on the corrosion rates and changes in the solution pH values have been ignored. The pH variation in implanted microenvironments is a major concern. Plasma pH is normally 7.2-7.4. When the pH value rises or falls beyond normal levels, however, a number of adverse

effects may occur.

In physiological biomaterial evaluation, in vivo corrosion tests are considerably time-consuming, with in vitro corrosion tests being more convenient and economical during early-stage studies. First, the number of animals used and the duration of animal experiments can be reduced significantly [37]. Second, the physiological environment of each patient and the location of his or her implants are unique and vary over time. However, in vitro corrosion studies performed in physiological solutions with changing components and concentrations have remained inconclusive [7, 8, 11]. Therefore, the corrosion resistance of magnesium alloys in physiological environments must be evaluated more extensively to gain further insight into the degradation mechanisms inside the human body.

To the best of our knowledge, the effects of bicarbonate, hydrogen phosphate, dihydrogen phosphate and sulphate anions in saline solutions on the bio-corrosion behaviour of magnesium alloys are unknown. Although magnesium alloys are promising for dental implants, the pH value of the food or diet does not change significantly in the mouth. Bicarbonate ions are present in the carbonated water typically found in soft drinks and carbonated beverages, which are consumed heavily during the summer. However, the impact of bicarbonate ions on the bio-corrosion of magnesium alloys is still far from being understood.

This study aims to determine the influence of bicarbonate, sulphate, hydrogen phosphate and dihydrogen phosphate ions at three concentrations in saline solution on the corrosion of magnesium alloy AZ31 and better understand the influence of solution pH on the corrosion of

magnesium alloys. The investigation will focus on the influence of HCO_3^- ions.

2. Experimental

2.1 Materials

A 230 mm × 1.2 mm commercial rolled magnesium alloy AZ31 (nominal composition: 2.5-3.0 wt% Al, 0.7-1.3 wt% Zn, >0.2 wt% Mn, Bal. Mg) sheet supplied by Beijing Guangling Jinghua Science and Technology Co., Ltd., was used in this study. The immersion samples were cut into pieces (10 mm × 10 mm × 1.2 mm). For the microstructural observation, the samples were ground with abrasive papers up to 2000 grit, polished with 1-μm diamond paste to a mirror finish and etched in a solution containing 5 ml of HNO_3, 3 ml of ethanol and 100 ml of water and examined via optical microscopy. The grain size was evaluated using the linear intercept method according to ASTM E122-88. The average grain size was acquired by counting the number of grains intercepted by five straight lines sufficiently long to yield at least 50 intercepts [24, 38]. The sample surface was also ground to 2000 grit for the electrochemical, immersion and evolution tests before being ultrasonically cleaned in an acetone solution and dried in warm air.

2.2 Hydrogen evolution and pH measurements

The volume of hydrogen gas released during the immersion depended on the dissolution of magnesium. The anodic reaction proceeded as follows:

$$Mg \rightarrow Mg^{2+} + 2e^- \qquad (1)$$

The cathodic reaction proceeded as follows:

$$2H_2O + 2e^- \rightarrow 2OH^- + H_2 \uparrow \qquad (2)$$

Thus, the total reaction combined the above two reactions:

$$Mg + 2H_2O \rightarrow Mg(OH)_2 + H_2 \uparrow \qquad (3)$$

Therefore, the corrosion rate of magnesium may be monitored by the volume of hydrogen evolved per unit time and area. The hydrogen evolution rate (HER) is expressed as [38]

$$HER = \frac{V}{St} \qquad (4)$$

where S is the exposed area, t is the immersion time and V is the volume of hydrogen evolution. The HER plotted against the immersion time reflects the kinetic change in the hydrogen evolution, which is affected by the corrosion products formed on the magnesium alloys.

A graduated cylinder was inverted in a beaker inside a digitally controlled water bath maintained at 37 ± 0.5 ºC. The ratio of solution volume (ml) to sample area (cm^2) was 25:1. The samples (25 mm × 25 mm × 1 mm) were immersed in 310 ml of solution for 10 h, and the evolved hydrogen volumes were recorded hourly.

Saline solution was chosen, and the solution pH was not controlled for simplicity and to avoid disturbing the anions of interest [11]. As listed in Table 1, 13 solutions were prepared using NaCl, $NaHCO_3$, $MgSO_4 \cdot 7H_2O$, $Na_2HPO_4 \cdot 12H_2O$ and KH_2PO_4, and their concentrations (Table 1) were set according to their levels in Hank's solution.

Monitoring the pH values in chemical and biological environments is critical. The pH values steadily increased during the dissolution of magnesium according to reaction (3). The pH was measured in 56-ml solutions for the smaller samples (10 mm × 10 mm × 1 mm) with a exposed area of 1.4 cm^2 according to a ratio of solution volume (ml) to sample area (cm^2) of 40:1 in

hydrogen evolution at 37 ± 0.5 ºC with a digital glass electrode pH meter (PHS–25). This pH meter was calibrated before each measurement. Three samples were measured for each test.

2.3 Electrochemical tests

A potentiostat (EG & G, 273) was utilised to study the electrochemical corrosion behaviour. A three-electrode system was used: the working electrode had an exposed surface area of 2.84 cm^2, and a saturated calomel electrode (SCE) and platinum plate were used as the reference and auxiliary electrodes, respectively. The polarisation measurements began after the samples had soaked in the solutions for 5 min. The potential was scanned from -300 mV to +300 mV relative to the SCE versus the open-circuit potentials (OCPs) at a scan rate of 0.5 mV/s. The tests were performed in a water bath at 37 ± 0.5 ºC. The samples were measured in triplicate to ensure reproducibility.

2.4 Surface analysis

The samples were removed after 10 h of immersion in various solutions and ultrasonically cleaned in acetone solution. The corrosion morphologies and structures of the samples were examined using scanning electron microscopy (SEM, KYKY-2800B) and X-ray diffraction (XRD, D/Max2500PC) with a Cu $K_{\alpha 1}$ (λ = 0.15406 nm) source operated at 30 kV and 100 mA.

3. Results

3.1 Microstructural observation

Fig. 1 shows the three-dimensional optical microstructure of the rolled AZ31 alloy. The microstructure is characterised by a fine-grained α-Mg matrix and Al-Mn intermetallics, which appear as black dots in the image [22, 27]. The average grain size is 6.4 μm in the sectional view,

which is perpendicular to the rolling direction. The extremely refined microstructure with equiaxed grains indicates that dynamic recrystallisation occurred during the rolling process. There is no $Mg_{17}Al_{12}$ phase present in the alloy, but some AlMn particles, such as Al_6Mn or Al_8Mn_5, may be present at the grain boundaries or inside the grains (Fig. 1) [22].

3.2 Influence of various anions on the hydrogen evolution rate

The hydrogen evolution rates (HERs) for the AZ31 alloys are plotted against immersion time in the various solutions in Fig. 2. The influence of these anions on the HER varied by the species present and its concentration. The HER decreased as the immersion time increased before stabilising. This behaviour may be attributed to the layer of corrosion products that precipitated on the surface of the alloy.

Generally, the HERs decreased as the bicarbonate, hydrogen phosphate and dihydrogen phosphate concentrations decreased and the sulphate concentration increased (Fig. 2). Compared to the saline solution (solution 1), the HER was lower for a bicarbonate concentration of 4.2 mmol/L but higher for concentrations of 8.3 mmol/L and above (Fig. 2a). Fig. 2b shows the influence of sulphate ions on the HER. At a concentration of 4.8×10^{-4} mol/L, the sulphate ions had no influence on the HER. However, the HER was faster than that in the saline solution when the sulphate content was below this level and slower when the sulphate content was above this level. This result may be related to pH changes and the formation of the corrosion product film.

Interestingly, the HERs were always lower in the presence of phosphate and chloride ions than in saline solution (Fig. 2c-d). Furthermore, the HER decreased with increasing HPO_4^{2-} and $H_2PO_4^-$

concentrations. However, after 10 h of immersion, there was no significant distinction between the HERs measured in the presence of HPO_4^{2-} ions. Thus, the HPO_4^{2-} concentration had no obvious impact on the corrosion rate due to the formation of a compact and protective corrosion product film.

3.3 Influence of various anions on the solution pH

Fig. 3 lists the pH changes of the solutions as a function of immersion time. The pH of the saline solution increased abruptly from 8.5 to 9.4 (solution 1) after 2 h of immersion, followed by a drop (Fig. 3a). This result was attributed to the dissolution of magnesium and the subsequent formation of magnesium hydroxide. Upon the addition of bicarbonate ions to the saline solution, the pH initially increased abruptly and then slowly increased with further immersion time (Fig. 3a). Meanwhile, the pH of the solutions in the presence of bicarbonate and chloride ions decreased as the bicarbonate concentration increased.

Adding sulphate ions to the saline solutions rapidly increased the pH values (Fig. 3b), with the values far exceeding those of saline solutions with and without bicarbonate ions. After 2 h of immersion, the pH values gradually declined. The pH values also decreased as the sulphate concentration increased.

As indicated by Fig. 3c-d, the hydrogen phosphate and dihydrogen phosphate ions also increased the pH values. However, the pH values of the saline solution exceeded those of every phosphate-containing solution (solutions 8-13) after 2 h of immersion. Interestingly, the pH values decreased considerably as the concentrations of both hydrogen phosphate and dihydrogen

phosphate ions increased.

Thus, the influence exerted by the pH when the above anions were present declined as follows: sulphate > hydrogen phosphate > dihydrogen phosphate > bicarbonate.

3.4 Influence of various anions on electrochemical behaviour

During the early stages of immersion, the open-circuit potential (OCP) first increased rapidly and then tended to stabilise (Fig. 4a). The OCP was clearly higher in the presence of chloride ions than in the presence of both chloride and bicarbonate ions. Therefore, the bicarbonate ions significantly reduced the OCPs of the alloys as the bicarbonate concentration increased. The sudden drop in the OCP after 14.1 min with chloride ions corresponded to the breakdown of the oxide film of the alloy. Additionally, the fluctuations in the OCP curves measured in the presence of bicarbonate and chloride ions (Fig. 4a) implied the breakdown of the oxide film and the formation of corrosion pits and $Mg(OH)_2$ precipitate.

The polarisation curves for the AZ31 alloys in the presence of bicarbonate and chloride ions are depicted in Fig. 4b. The bicarbonate ions shifted the anodic polarisation behaviour but slightly decreased the corrosion resistance of the alloy. A passivity region and a breakdown potential (E_b) were observed in the anodic branches due to the formation of carbonate-containing films.

Fig. 5a displays the OCP versus time curves obtained when both sulphate and chloride ions were present. The curves were similar to one another, implying that the oxide film had dissolved and the protective corrosion product layer had formed. The reduction in OCPs was smaller in the presence of sulphate ions than in the presence of hydrogen carbonate (Fig. 4a), hydrogen

phosphate (Fig. 6a) or dihydrogen phosphate (Fig. 7a) ions. Sulphate ions impacted the corrosion rates less strongly as the concentration increased because the cathodic branches remained unchanged, except for the case of solution 5 (Fig. 5b). The presence of sulphate and chloride ions changed the anodic polarisation behaviour of the alloy. For example, for the solution containing 0.48 mmol/L sulphate ions, the breakdown potential (E_b) was -1362 mV/SCE, or 151 mV /SCE higher than its OCP.

Similar to the case of bicarbonate and sulphate ions, the hydrogen phosphate and dihydrogen phosphate ions also lowered the OCPs of the alloy, as depicted in Fig. 6a and Fig. 7a. However, the presence of hydrogen phosphate and dihydrogen phosphate ions shifted the cathodic polarisation curves toward the left and the anodic polarisation curves toward the right (Fig. 6b and 7b). Accordingly, the corrosion current density of the alloy when chloride was present along with hydrogen phosphate and dihydrogen phosphate ions was lower than that in the presence of only chloride ions. This behaviour was attributed to the prevention of cathodic hydrogen evolution due to the formation of phosphate precipitates.

3.5 Influence of anions on corrosion morphologies

Conspicuous, localised corrosion occurred on the surface, featuring traces consistent with filiform corrosion. A corrosion product layer of $Mg(OH)_2$ precipitate formed after 1 h of immersion in saline solution (Fig. 8a). After 2 h of immersion, the precipitated $Mg(OH)_2$ layer became more uniform and thicker (Fig. 8b). After 3 h of immersion, the corroded area expanded (Fig. 8c). Finally, after 10 h of immersion, the specimen was subjected to a serious attack along the scratch markings, and the surface became rough (Fig. 8d). Corrosion pits appeared due to the

galvanic corrosion between the anodic α-Mg matrix and the cathodic Al-Mn particles [39]. The scratch markings produced during grinding were the active sites for the initial corrosion. The corrosion morphology was similar to that of ultra-high-purity Mg in 3.5% NaCl solution saturated with $Mg(OH)_2$ [21] and field-exposed AZ31 alloy in a tropical marine environment [15].

Fig. 9 presents the corrosion morphologies after immersion in the presence of the various anions for 10 h. The inset shows the corresponding high-magnification SEM image. Clearly, more severe attacks occurred in solutions 3 (Fig. 9b) and 4 (Fig. 9c) than in solution 2 (Fig. 9a) in the presence of bicarbonate ions. Filiform corrosion initiated on the alloy as it soaked in solution 2. However, overall corrosion occurred in solutions 3 and 4 (Fig. 9b-c).

Additionally, filiform corrosion (Fig. 9d, 9e) and general corrosion (Fig. 9f-l) occurred in the presence of sulphate (Fig. 9d-f), hydrogen phosphate (Fig. 9g-i) and dihydrogen phosphate (Fig. 9j-l) ions. In particular, the presence of higher concentrations of phosphate ions (Fig. 9i, 9l) caused the formation of a bamboo-like compact layer of corrosion products, leading to a lower corrosion rate. This layer may have been formed by the dehydration of the corrosion product layer after drying in air [7].

3.6 XRD results

Fig. 10 displays the XRD patterns of the samples after immersion in various solutions for 10 h. When the magnesium alloy was soaked in saline solution, reaction (3) occurred. This reaction gave rise to an increase in pH and the formation of magnesium hydroxide and aluminium hydroxide [11]. In the presence of bicarbonate, insoluble magnesium carbonate, $MgCO_3$, may precipitate on the sample surface as the local pH near the surface increases, reaching 9.3 [13].

$MgCO_3$ is more stable at higher [HCO_3^-] relative to $Mg(OH)_2$ [7]. Thus, the corrosion products included magnesium hydroxide and magnesium carbonate. Similarly, in the presence of hydrogen phosphate and dihydrogen phosphate, insoluble magnesium phosphate formed [7]. However, magnesium phosphate was not observed in Fig. 10, possibly because the corrosion product layer was too thin to detect. In contrast, in the presence of sulphate, magnesium sulphate, $MgSO_4$ and its hydrates ($MgSO_4 \cdot xH_2O$ (x = 3, 6, 7)) was discerned.

4. Discussion

Fig. 11 depicts the HERs after 10 h of exposure to the solutions**.** The HER increased with increasing concentration of bicarbonate ions. In contrast, the HER decreased with increasing concentration of sulphate ions. Moreover, the HERs in saline solution with 0.48 mmol/L and 0.81 mmol/L $MgSO_4 \cdot 7H_2O$ were lower than that in saline solution without additives. Relative to saline solution, the HER decreased in the presence of hydrogen phosphate and dihydrogen phosphate. However, the HER in presence of hydrogen phosphate was much lower than that in presence of dihydrogen phosphate. The effect of the hydrogen phosphate concentration on HER was insignificant, whereas the HER increased significantly as the dihydrogen phosphate concentration increased.

Furthermore, the HER was slightly different from the corresponding current density, as shown in Fig. 12. The current density obtained from the Tafel plots for the potentiodynamic polarisation curves was not in agreement with the HERs of the corresponding samples because of the limitations of the polarisation curves applied to characterise the corrosion rate of the magnesium alloys [40-41]. The anodic polarisation curve of magnesium and its alloys did not obey the Tafel

law [40-41]. It has been reported that the electrochemical measurements of the corrosion rate, which are based on the corrosion current density, did not agree with the direct measurements evaluated from the evolved hydrogen [42]. Thus, the current density was usually inconsistent with the HER.

4.1 Relationship between the solution pH and HER

The pH increase in the presence of chloride revealed that magnesium hydroxide films formed on the AZ31 alloy (Fig. 8a). After an immersion time of 14.1 min, a decrease in the OCP values (Fig. 4a) indicated that the $Mg(OH)_2$ film dissolved by reacting with the chloride ions.

$$Mg(OH)_2 + 2Cl^- \rightarrow MgCl_2 + 2OH^- \quad (5)$$

As a result, corrosion pits and filiform corrosion were observed on the samples, as illustrated in Fig. 8. The relationship between the concentration of Mg^{2+} ions, $[Mg^{2+}]$, and pH was constructed using reference [43].

$$Log[Mg^{2+}] = 16.95 - 2pH \quad (6)$$

For the solution saturated with Mg^{2+} ions, the concentration of Mg^{2+} ions [43] is

$$[Mg^{2+}] = 10^{-3.90} \quad (7)$$

Inserting Eq. (7) into Eq. (6) yields

$$pH = 10.43. \quad (8)$$

Thus, 10.43 was designated as the pH of the solution saturated with Mg^{2+} ions [21, 44].

Based on reactions (1)-(3), the change in $[Mg^{2+}]$ with immersion time also reflects the corrosion rate for magnesium and its alloy. Fig. 13 presents the variations in $[Mg^{2+}]$ and pH relative to the immersion time for the AZ31 alloy in solution 1. It is known that the $[Mg^{2+}]$ at saturation is $1.26 \times$

10^{-4} mol/L [44]. It is evident from Fig. 13 that the pH value peaked (at approximately 10.4) as the Mg^{2+} ions in the solution reached saturation after 1 h of immersion [44]. Compared to the HER results (Fig. 2), there was a significant distinction between the changes in [Mg^{2+}] and the HER. Specifically, the HER decreased continuously with increasing immersion time. However, [Mg^{2+}] did not always decrease; it increased steadily after 4 h of immersion. This novel finding revealed the dissolution processes of the $Mg(OH)_2$ precipitates, which occurred via reaction (5) with chloride ions.

Interestingly, the change in the solution pH (Fig. 14) is not in complete accordance with its corresponding HER (Fig. 2). For example, in the presence of hydrogen phosphate and dihydrogen phosphate ions, the solution pH was low, but the alloy also had a low HER. The solution pH decreased significantly with the concentrations of bicarbonate, sulphate, hydrogen phosphate and dihydrogen phosphate ions after 10 h of immersion. Only the pH values of the solution with 0.24 mmol/L and 0.48 mmol/L sulphate ions were higher than that of the saline solution, which was due to the lack of dissociation of hydrogen ions from sulphate ions into the solution. Therefore, when chloride and the other anion species were present, the change in the solution pH was not related to its corresponding corrosion rate due to the differences between the initial solution pH values generated by the anions.

4.2 Influence of bicarbonate ions on the formation mechanism of the corrosion product layer

The stability of the corrosion product film depended on the solution pH. Higher solution pH values made the magnesium surface film more passive [44]. Moreover, the stability of $MgCO_3$ also depended on the bicarbonate ion concentration. Although the solubility product constant (K_{sp})

(Table 2) [45] of $MgCO_3$ was six orders of magnitude greater than that of $Mg(OH)_2$ [46], the $MgCO_3$ layer was more stable at higher [HCO_3^-] than the $Mg(OH)_2$ layer was [7]. The stable zone for $MgCO_3$ in the log [Mg^{2+}]-pH plot widened as [HCO_3^-] increased [7].

Because the presence of bicarbonate ions in saline solution increased the solution pH values, as demonstrated in Fig. 3, bicarbonate ion hydrolysis was possible [15]:

$$HCO_3^- + H_2O \leftrightarrow H_2CO_3 + OH^- \quad (9)$$

According to reaction (4), hydroxide ions were produced as magnesium alloys were exposed to the chloride-bearing aqueous solution. The continuous increase in the concentration of hydroxide ions, [OH^-], generated variations in the corrosion products. This process occurred in three stages:

(I) During the initial period, [Mg^{2+}] and [OH^-] were relatively low. Fig. 14 reveals that the [Mg^{2+}] in the saline solution always exceeded the saturation value (1.02×10^{-4} mol/L), indicating the formation of $Mg(OH)_2$ precipitates. However, when bicarbonate ions were present, magnesium carbonate species, such as $MgCO_3 \cdot xH_2O$ (x = 3, 5) [15, 22] and $(Mg_5(CO_3)_4(OH)_{2.5}H_2O$ [45-47], were more stable than magnesium hydroxide; therefore, the magnesium carbonate hydrates formed preferentially [15, 22]:

$$Mg^{2+} + HCO_3^- + OH^- + (x\text{-}1)H_2O \leftrightarrow MgCO_3 \cdot xH_2O \ (x = 3, 5) \quad (10)$$

The relationship between [Mg^{2+}] ions and [HCO_3^-] ions is subsequently established [7]:

$$\text{Log } [Mg^{2+}] + \log[HCO_3^-] = 5.3 - \text{pH} \quad (11)$$

Based on Eq. (11), the variations in [Mg^{2+}] + [HCO_3^-] relative to the immersion time are plotted in Fig. 15.

Interestingly, Fig. 15 features a turning point (A). During the first hour of immersion, $[Mg^{2+}]$ + $[HCO_3^-]$ decreased in the following order: solution 2 > solution 3 > solution 4. The films thickened as the bicarbonate ion concentration increased [36]. Additionally, micro cracks formed on the surface during the dry processing. However, after 1 h of immersion, the $[Mg^{2+}]$ + $[HCO_3^-]$ decreased in the opposite sequence: solution 4 > solution 3 > solution 2. This scenario was attributed to the rapid increase in solution pH caused by the chloride ions, which generated the highest pH value (9.4) after 2 h in the presence of chloride ions (Fig. 3a).

The total concentration of magnesium and bicarbonate ions ($[Mg^{2+}]$ + $[HCO_3^-]$) declined markedly with increasing immersion time because of the formation of a protective magnesium carbonate and/or magnesium hydroxide film, as indicated by Fig. 16a-c. During the initial immersion, magnesium carbonate precipitated on the surface, and fewer pits were observed (Fig. 16a-c). During subsequent immersions, more corrosion pits were observed in solutions 3 (Fig. 16e, h) and 4 (Fig. 16f, i). The solution pH decreased as the bicarbonate concentration increased. Specifically, the pH of solution 2 was higher than those of solutions 3 and 4 (Fig. 3), creating a dense layer of corrosion product film over time (Fig. 16a, d, g). Thus, the HER of solution 2 was lower than that of solution 1 based on the corrosion morphologies observed in Fig. 8a-c.

(II) During the second period, $[Mg^{2+}]$ and $[OH^-]$ increased continuously, but the concentration of bicarbonate ions decreased. Therefore, magnesium hydroxide and magnesium carbonate were produced simultaneously due to their similar solubilities.

$$2Mg^{2+} + CO_3^{2-} + 2OH^- \leftrightarrow Mg(OH)_2\downarrow + MgCO_3\downarrow \qquad (12)$$

These precipitates were verified by their XRD patterns (Fig. 10), and analogous results have

been reported by Jang [36]. Jang demonstrated that the corrosion products of the AZ31 alloy were mainly $Mg(OH)_2$ and $Mg_{0.833}Al_{0.167}(OH)_2](CO_3)_{0.083}\cdot 0.75H_2O$ after immersion tests in 103 mmol/L NaCl and 27 mmol/L Na_2CO_3 over 10 days.

(III) During the final period, $[Mg^{2+}]$ and $[OH^-]$ increased continuously, while $[HCO_3^-]$ decreased and was completely consumed. Consequently, only magnesium hydroxide formed.

The corrosion pits observed in Fig. 16e-f and Fig. 16h-i indicated that the precipitated $Mg(OH)_2$ had dissolved through reaction with the chloride ions.

Further investigations are necessary to describe the transition from $MgCO_3$ to $MgCO_3$ + $Mg(OH)_2$, eventually leading to $Mg(OH)_2$.

The corrosion morphology of magnesium alloys is affected by the $[HCO_3^-]$ [46]. Gulbrandsen [48] noted that the corrosion rate of magnesium was related to the HCO_3^- concentration, contributing to the quality of the film covered by the corrosion products. The microphotographs displayed in Fig. 9a revealed that either pitting or filiform corrosion may occur depending on $[HCO_3^-]$ in the saline solutions. Xin [11] suggested that the HCO_3^- ions could induce rapid surface passivity when magnesium carbonate precipitated and completely suppressed the pitting corrosion. For $[HCO_3^-] > 12$ mmol/L, the $MgCO_3$ film inhibited the pitting corrosion [11]. For $[HCO_3^-] < 12$ mmol/L, the pitting corrosion was not prevented.

Jang [36] reported that bicarbonate accelerated the overall corrosion rate as its concentration increased. However, this result does not agree with our finding. In this study, when $[HCO_3^-] <$ 8.33 mmol/L, HER decreased; however, when $[HCO_3^-] \geq 8.33$ mmol/L, the bicarbonate accelerated HER as its concentration increased.

Based on the above discussion, the formation of $MgCO_3$ precipitates in the bicarbonate-bearing saline solutions is schematically illustrated in Fig. 17.

The complicated formation process may be a cyclic system with six steps:

(1) The electrochemical dissolution of magnesium and the donation of electrons (Eq. 1).

(2) Water-induced decomposition by electron capture and hydrogen evolution (Eq. 2).

(3) The hydrolysis of bicarbonate (Eq. 9).

(4) The formation of magnesium carbonate (Eq. 10 and 12).

(5) The formation of magnesium hydroxide (Eq. 3).

(6) The dissolution of magnesium hydroxide through a reaction with chloride (Eq. 5).

This process may explain the bicarbonate-dependent acceleration of the dissolution of the magnesium alloys.

4.3 Influence of sulphate ions

For the SO_4^{2-} ions, the passivation observed in the anodic polarisation curves can be explained by the literature data [49, 50]. Previous reports revealed that the surface films contained mostly $Mg(OH)_2$ and grow rapidly after immersion in the test solutions; the thickness of the films exceeded 70 nm and 12 μm within 60 s [51] and 21 h [52] of immersion in 0.1 M Na_2SO_4, respectively. Other studies [42, 47, 51-52] disclosed that protective and compact films, including $Mg(OH)_2$ and $MgAl_2(SO_4)_4 \bullet 22H_2O$, form on die-cast AZ91D surfaces in both NaCl and Na_2SO_4 solutions. Światowska [47] demonstrated that corrosion pits occur on pure magnesium surfaces in sulphate solutions. Ardelean [16] confirmed a low-intensity signal (SO_4^-) corresponding to sulphates detected by ToF-SIMS but not by XPS for Mg-Y-Nd-Zr alloys immersed in Na_2SO_4.

During this study, the intensity of the XRD signal probed on the corroded surface was weak, indicating that the major corrosion product was $Mg(OH)_2$. Severe pitting corrosion was observed on the samples (Fig. 9g-f). Sulphate ions accelerated the HERs.

4.4 Influence of hydrogen phosphate and dihydrogen phosphate ions

For the phosphate-containing solution, the polarisation plots in Fig. 6b and Fig. 7b demonstrate the activation-controlled corrosion of the alloy. The reduction in the corrosion current density was ascribed to the precipitation of magnesium phosphate.

$$H_2PO_4^- \rightarrow HPO_4^{2-} + H^- \quad (13)$$

$$HPO_4^{2-} \rightarrow PO_4^{3-} + H^- \quad (14)$$

$$3Mg^{2+} + 4OH^- + 2H_2PO_4^- + (n\text{-}4)\ H_2O \rightarrow Mg_3(PO_4)_2 \cdot n\ H_2O \quad (15)$$

$$3Mg^{2+} + 4OH^- + 2HPO_4^{2-} + (n\text{-}2)\ H_2O \rightarrow Mg_3(PO_4)_2 \cdot n\ H_2O \quad (16)$$

Fig. 9g-l confirms that a protective and compact corrosion product layer formed after 10 h of immersion in the phosphate solutions. These results agree with Jang's report [36]; phosphate induced the formation of a densely packed, amorphous magnesium phosphate corrosion product layer when HPO_4^{2-} and Cl^- were present. This layer slowed the corrosion rate of AZ31 and prohibited pitting corrosion. In addition, Xin [11] demonstrated that HPO_4^{2-} ions significantly delayed the pitting corrosion.

5. Conclusions

(1) The hydrogen evolution rate decreased with decreasing bicarbonate, hydrogen phosphate and dihydrogen phosphate concentrations and increasing sulphate concentration. The corrosion rate decreased in saline solution with a lower [HCO_3^-] and higher [SO_4^{2-}] but improved when

[HCO_3^-] and [SO_4^{2-}] were higher and lower, respectively. The presence of hydrogen phosphate and dihydrogen phosphate ions significantly reduced the corrosion rate of the alloy. The presence of bicarbonate, sulphate, and hydrogen phosphate as well as dihydrogen phosphate ions significantly decreased the open-circuit potential of AZ31.

(2) The anions significantly impacted the formation and stability of the corrosion product film. The process and formation mechanism of the magnesium carbonate film were elucidated, and a corresponding model was proposed.

(3) The change in the solution pH was not related to the corresponding corrosion resistance due to the differences between the initial solution pH values generated by the anions.

Acknowledgements

This work was supported by National Natural Science Foundation of China (51241001) and Natural Science Foundation of Shandong Province (ZR2011EMM004), the Open Foundation of State Key laboratory for Corrosion and Protection (SKLCP2012KF03), Taishan Scholarship Project of Shandong Province (TS20110828).

References

[1] R.C. Zeng, W. Dietzel, F. Witte, N. Hort, The progress and challenge for magnesium alloys as biomaterials, Adv. Eng. Mater.10(2008) B3-B14.

[2] M.P. Staiger, A.M, Pietak, J. Huadmai, G. Dias, Magnesium and its alloys as orthopedic biomaterials: A review, Biomaterials 27(2006)1728-34.

[3] G. Song, Control of biodegradation of biocompatible magnesium alloys, Corros. Sci. 49(2007)1696–701.

[4] F. Witte, V. Kaese, H. Haferkamp, E. Switzer, A. Meyer-Lindenberg, C.J. Wirth, H. Windhagen, In vivo corrosion of four magnesium alloys and the associated bone response, Biomaterials 26(2005)3557-63.

[5] P. Zartner, R. Cesnjevar, H. Singer, M. Weyand, First successful implantation of Biodegradable metal stent into the left pulmonary artery of a preterm baby, Catheter. Cardio. Inte. 66(2005)590-4.

[6] A. Krause, N. von der Hoeh, D. Bormann, C. Krause, F. W. Bach, H. Windhagen, A. Meyer-Lindenberg, Degradation behaviour and mechanical properties of magnesium implants in rabbit tibiae, J. Mater. Sci. 45(2010) 624–32.

[7] L. Wang, T. Shinohara, B.P. Zhang, Influence of chloride, sulphate and bicarbonate anions on the corrosion behavior of AZ31 magnesium alloy, J. Alloys Compd. 496(2010)500-7.

[8] X.N. Gu, Y.F. Zheng, L.J. Chen, Influence of artificial biological fluid composition on the biocorrosion of potential orthopedic Mg-Ca, AZ31, AZ91 alloys, Biomed. Mater. 4(2009) 065011.

[9] C.L. Liu, Y.C. Xin, X.B. Tian, P.K. Chu, Degradation susceptibility of surgical magnesium alloy in artificial biological fluid containing albumin, J. Mater. Res. 22(2007)1806-14.

[10] R.C. Zeng, J. Chen, W. Dietzel, N. Hort, K.U. Kainer, Electrochemical behavior of magnesium alloys in simulated body fluids, Trans. Nonferrous Met. Soc. China 17(2007)s166-9.

[11] Y. Xin, K. Huo , H. Tao , G. Tang, P.K. Chu, Influence of aggressive ions on the degradation behavior of biomedical magnesium alloy in physiological environment, Acta

Biomater. 4(2008)2008-15.

[12] A. Yamamoto, S. Hiromoto, Effect of inorganic slats, amino acids and proteins on degradation of pure magnesium in vitro, Mater. Sci. Eng. C 29(2009)1559-68.

[13] F. Witte, J. Fischer, J. Nellesen, H.A. Crostack, V. Kaese, A. Pisch, F. Beckmann, H. Windhagen, In vitro and in vivo corrosion measurements of magnesium alloys, Biomaterials 27(2006)1013-8.

[14] S. Feliu Jr., A. Samaniego, A.A. El-Hadad, I. Llorente, The effect of $NaHCO_3$ treatment time on the corrosion resistance of commercial magnesium alloys AZ31 and AZ61 in 0.6 M NaCl solution, Corros. Sci. 67(2013)204-16.

[15] Z. Cui, X. Li, K. Xiao, C. Dong, Atmospheric corrosion of field-exposed AZ31 magnesium in a tropical marine environment, Corros. Sci. 76(2013)243-56.

[16] H. Ardelean, A. Seyeux, S. Zanna, F. Prima, I. Frateur, P. Marcus, Corrosion processes of Mg–Y–Nd–Zr alloys in Na_2SO_4 electrolyte, Corros. Sci. 73(2013)196-207.

[17] M.B. Kannan, R.K.S. Raman, In vitro degradation and mechanical integrity of calcium-containing magnesium alloys in modified-simulated body fluid, Biomaterials 29(2008)2306-14.

[18] M. Liu, G. Song, Impurity control and corrosion resistance of magnesium–aluminum alloy, Corros. Sci. 77(2013) 143-50.

[19] H. Matsubara, Y. Ichige, K. Fujita, H. Nishiyama, K. Hodouchi, Effect of impurity Fe on corrosion behavior of AM50 and AM60 magnesium alloys, Corros. Sci. 66(2013)203-10.

[20] R. C. Zeng, J. Chen, W. Dietzel, R. Zettler, J. F. dos Santos, M. L. Nascimento, K. U. Kainer. Corrosion of friction stir welded magnesium alloy AM50, Corros. Sci. 51(2009)1738-46.

[21] F. Cao, Z. Shi, J. Hofstetter, P. J. Uggowitzer, G. Song, M. Liu, A. Atrens, Corrosion of ultra-high-purity Mg in 3.5% NaCl solution saturated with $Mg(OH)_2$, Corros. Sci. 75(2013) 78-99.

[22] J. Liao, M. Hotta, S. Motoda, T. Shinoharra, Atmospheric corrosion of two field exposed AZ31B magnesium alloys with different grain size, Corros. Sci. 71(2013)53-61.

[23] J. Liao, M. Hotta, N. Yamamoto, Corrosion behaviour of fine-grained AZ31B magnesium alloy, Corros. Sci. 61(2012)208-14.

[24] R.C. Zeng, K.U.Kainer, C. Blawert, W. Dietzel. Corrosion of an extruded magnesium alloy ZK60 component-The role of microstructural features, J. Alloy. Compd. 509(2011) 4462-69.

[25] G. Song, A. Atrens, M. Dargusch, Influence of microstructure on the corrosion of diecast AZ91D, Corros. Sci. 41(1999)249-73.

[26] D. Orlov, K.D. Ralston, N. Birbilis, Y. Estrin, Enhanced corrosion resistance of Mg alloy ZK60 by integrated extrusion and equal channel angular pressing, Acta Mater. 59(2011) 6176-86.

[27] R. Zeng, Z. Lan, L. Kong, Y. Huang, H. Cui. Characterization of calcium-modified zinc phosphate conversion coatings and their influences on corrosion resistance of AZ31 alloy, Surf. Coat. Technol. 205 (2011) 3347-55.

[28] J.H. Syu, J.Y. Uan, M.C. Lin, Z.Y. Lin, Optically transparent Li–Al–CO_3 layered double hydroxide thin films on an AZ31 Mg alloy formed by electrochemical deposition and their

corrosion resistance in a dilute chloride environment, Corros. Sci. 68(2013)238-48.

[29] L.P. Xu, F. Pan, G.N. Yu, L. Yang, E.L. Zhang, K. Yang, In vitro and in vivo evaluation of the surface bioactivity of a calcium phosphate coated magnesium alloy, Biomaterials 30(2009)1512–23.

[30] A. Pietak, P. Mahoney, G.J. Dias, M.P. Staiger, Bone-like matrix formation on magnesium and magnesium alloys, J. Mater. Sci.: Mater. Med. 19(2008)407–415.

[31] J.C. Gao, L.C. Li, Y. Wang, Surface modification on Mg by alkali-heat-treatment and its corrosion behaviors in SBF, Chin. J. Nonferrous Met. 14(2004)1508-13.

[32] Y.C. Xin, C.L. Liu, X.M. Zhang, G.Y. Tang, X.B. Tian, P.K. Chu, Corrosion behavior of biomedical AZ91 magnesium alloy in simulated body fluids, J. Mater. Res. 22(2007) 2004-11.

[33] L. Xu, G. Yu, E. Zhang, F. Pan, K. Yang, In vivo corrosion behavior of Mg–Mn–Zn alloy for bone implant application, J. Biomed. Mater. Res. A 83(2007)703–11.

[34] Y.C. Xin, T. Hu, P.K. Chu, Degradation behaviour of pure magnesium in simulated body fluids with different concentrations of HCO_3, Corros. Sci. 53(2011)1522-28.

[35] C.L. Liu, Y.J. Wang, R.C. Zeng, X.M. Zhang, W.J. Huang, P.K. Chu, In Vitro Corrosion Degradation Behaviour of Mg-Ca Alloy in the Presence of Albumin, Corros. Sci. 52(2010)3341-7.

[36] Y. Jang, B. Collins, J. Sankar, Y. Yun, Effect of biological relevant ions on the corrosion products formed on AZ31B alloy: Improved understanding of magnesium corrosion, Acta Biomater. 9 (2013) 8761–8770.

[37] T. Kokubo, H. Takadama, How useful is SBF in predicting in vivo bone bioactivity, Biomaterials 27(2006)2907-15.

[38] R.C. Zeng, L. Sun, Y.F. Zheng, H.Z. Cui, E.H. Han, Corrosion and characterisation of dual phase Mg-Li-Ca alloy in Hank's solution: the influence of microstructural features, Corros. Sci. 79(2014)69-82.

[39] R.C. Zeng, W.Q. Zhou, E.H. Han, W. Ke, Effect of pH values on as-extruded magnesium alloy AM60, Acta Metall. Sin. 41(2005)307-11.

[40] G. Song, A. Atrens, Understanding magnesium corrosion-a framework for improved alloy performance, Adv. Eng. Mater. 5(2003)837-58.

[41] Z.M. Shi, M. Liu, A. Atren, Measurement of the corrosion rate of magnesium alloys using Tafel extrapolation, Corros. Sci. 52(2010)579-88.

[42] M.C. Zhao, M. Liu, G.L. Song, A.Atrens. Influence of pH and chloride ion concentration on the corrosion of Mg alloy ZE41, Corros. Sci. 50(2008)3168-78.

[43] R.C. Zeng, J. Chen, W. Ke, E.H. Han, W. Dietzel, pH value in simulated occluded corrosion cell for magnesium alloys, Trans. Nonferrous Met. Soc. China 17(2007)s194-7.

[44] G. Song, A. Atrens, D. St John, J. Nairn, Y. Li, Electrochemical corrosion of pure magnesium in 1 N NaCl, Corros. Sci. 39(1997)855–75.

[45] X.J. Liu, Y.X. Zhu, F. Gao, Chemistry of Inorganic Elements, Second edition, Science Press, Beijing, 2011.

[46] R. Lindstrom, L.G. Johansson, G.E. Thompson, P. Skeldon, J.E. Svensson, Corrosion of magnesium in humid air, Corros. Sci. 46(2004)1141–58.

[47] J. Świątowska, P. Volovitch, K. Ogle, The anodic dissolution of Mg in NaCl and Na_2SO_4 electrolytes by atomic emission spectroelectrochemistry, Corros. Sci. 52(2010)2372-8.

[48] E. Gulbrandsen, Anodic behaviour of Mg in HCO^-_3/CO^{2-}_3 buffer solutions. Quasi-steady measurements, Electrochim. Acta 37(1992)1403-12.

[49] J. Chen, J.Q. Wang, E.H. Han, J.H. Dong, W. Ke, AC impedance spectroscopy study of the corrosion behavior of an AZ91 magnesium alloy in 0.1 M sodium sulphate solution, Electrochim. Acta 52(2007)3299–309.

[50] L.J. Yang, Y.H. Wei, L.F. Hou, D. Zhang, Corrosion behaviour of die-cast AZ91D magnesium alloy in aqueous sulphate solutions, Corros. Sci. 52(2010)345-51.

[51] G. Baril, N. Pébère, The corrosion of pure magnesium in aerated and deaerated sodium sulphate solutions, Corros. Sci. 43(2001)471-84.

[52] Y. Tian, L.J. Yang, Y.F. Li, Y.H. Wei, L.F. Hou Y.G. Li, R.I. Murakami, Corrosion behaviour of die-cast AZ91D magnesium alloys in sodium sulphate solutions with different pH values, Trans. Nonferrous Met. Soc. China 21(2011)912-20.

Figure captions

Fig. 1 Three-dimensional optical microstructure of the rolled AZ31 alloy. The black dots indicate AlMn particles.

Fig. 2 HERs for AZ31 in solutions (a) 2-4, (b) 5-7, (c) 8-10 and (d) 11-13.

Fig. 3 Change in pH vs. time for AZ31 in solutions (a) 2-4, (b) 5-7, (c) 8-10 and (d) 11-13.

Fig. 4 (a) OCP vs. immersion time and (b) polarisation curves for AZ31 in solutions 1-4.

Fig. 5 (a) Potential versus time and (b) polarisation curves for AZ31 in solutions 1 and 5-7.

Fig. 6 (a) Potential versus time and (b) polarisation curves for AZ31 in solutions 1 and 8-10.

Fig. 7 (a) Potential versus time and (b) polarisation curves for AZ31 in solutions 1 and 11-13.

Fig. 8 SEM images of the corrosion morphology of the alloys after (a) 1 h, (b) 2 h, (3) 3 h and (d) 10 h of immersion in solution 1. The lines are scratches due to the grinding treatment.

Fig. 9 SEM images of the corrosion morphologies of AZ31 after immersion for 10 h in solutions (a) 2, (b) 3, (c) 4, (d) 5, (e) 6, (f) 7, (g) 8, (h) 9, (i) 10, (j) 11, (k) 12 and (l) 13. The insets represent their magnitudes.

Fig. 10 XRD patterns of the AZ31 alloys after immersion for 10 h in various solutions.

Fig. 11 HERs after immersion for 10 h in various solutions.

Fig. 12 Current densities of the samples in various solutions.

Fig. 13 pH and magnesium ion concentration vs. time for the AZ31 alloy in solution 1.

Fig. 14 pH after immersion for 10 h in various solutions.

Fig. 15 Variation in $[Mg^{2+}] + [HCO_3^-]$ versus immersion time for solutions 2, 3 and 4.

Fig. 16 Corrosion morphologies for the samples after immersion for 1 h in solutions (a) 2, (b) 3 and (c) 4; 2 h in solutions (d) 2, (e) 3 and (f) 4; and 3 h in solutions (g) 2, (i) 3 and (j) 4.

Fig. 17 Schematic illustration of the $MgCO_3$ precipitates forming in the presence of bicarbonate and chloride ions.

Table captions

Table 1 Chemical composition of the solutions used, mmol/L

Table 2 Solubility product constant (K_{sp}) values at 25 °C [45]

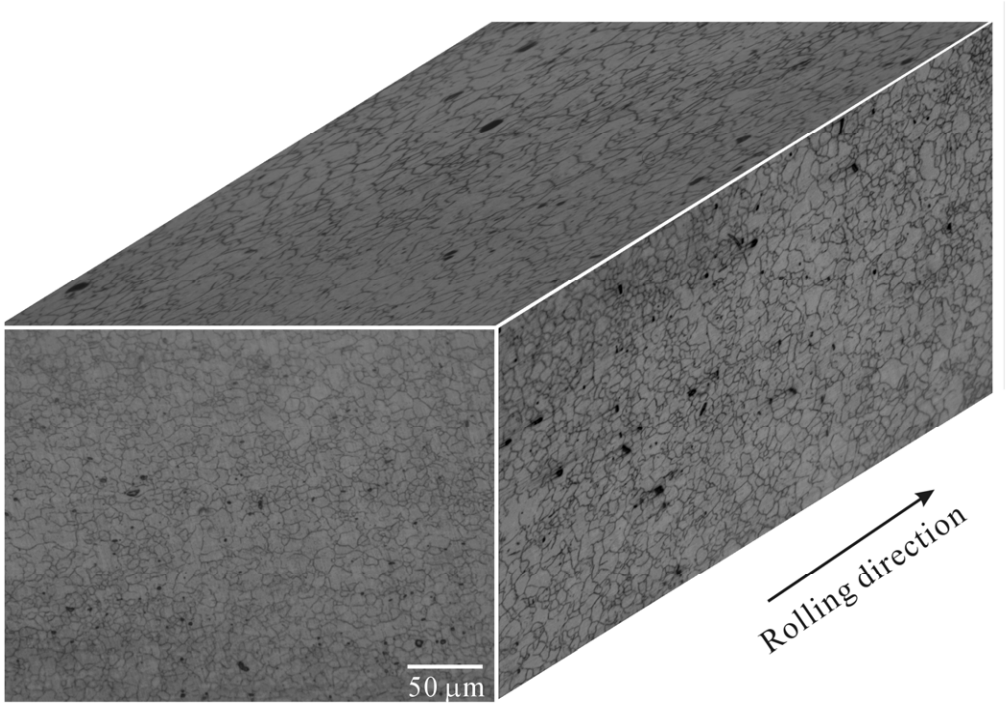

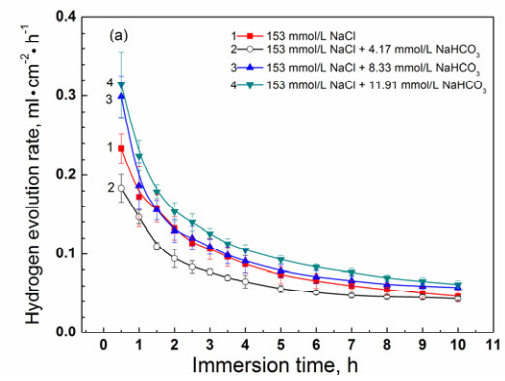

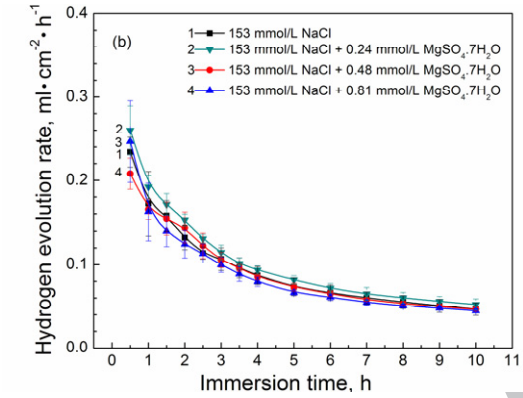

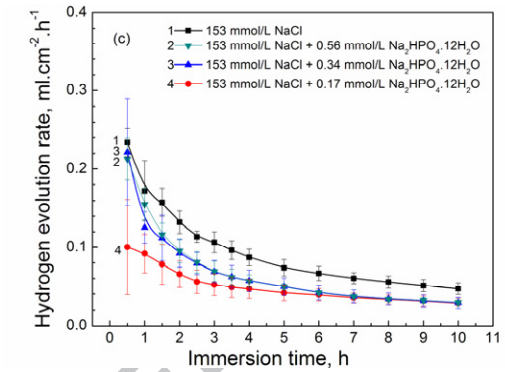

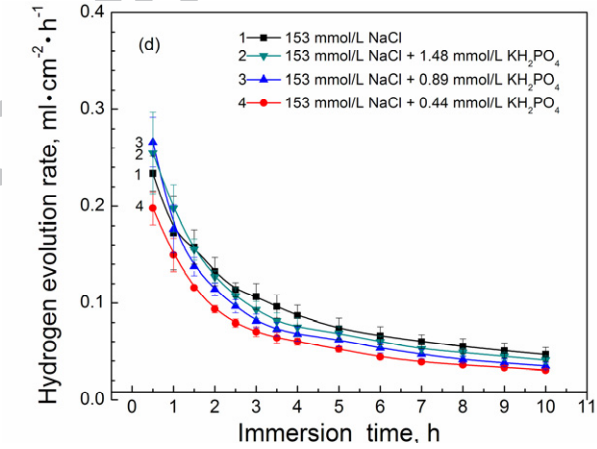

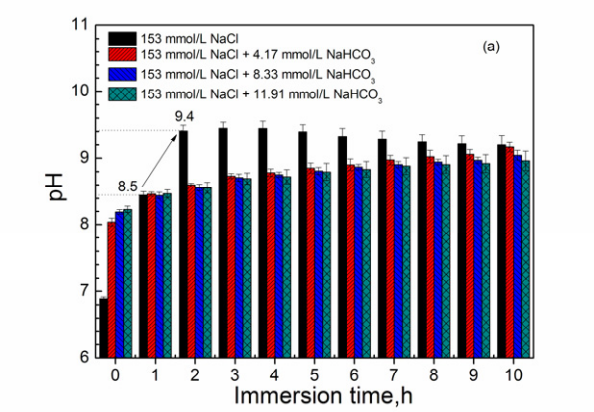

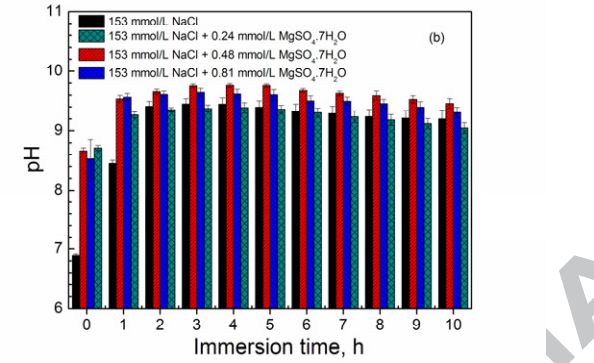

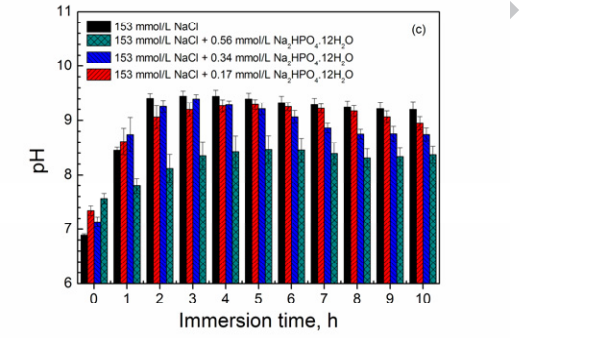

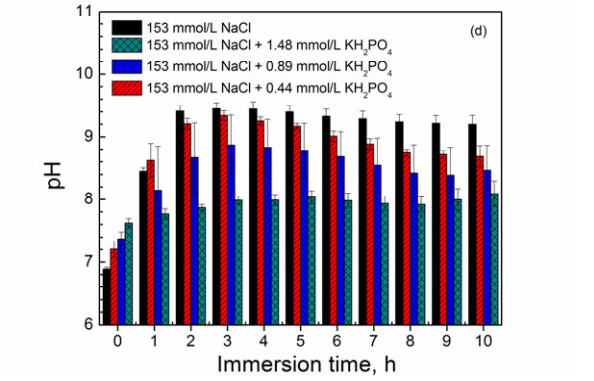

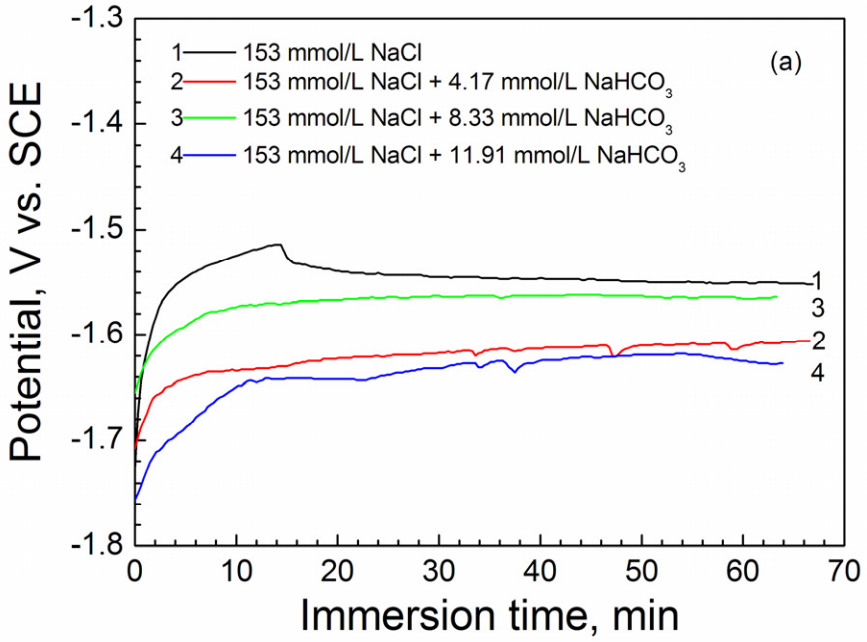

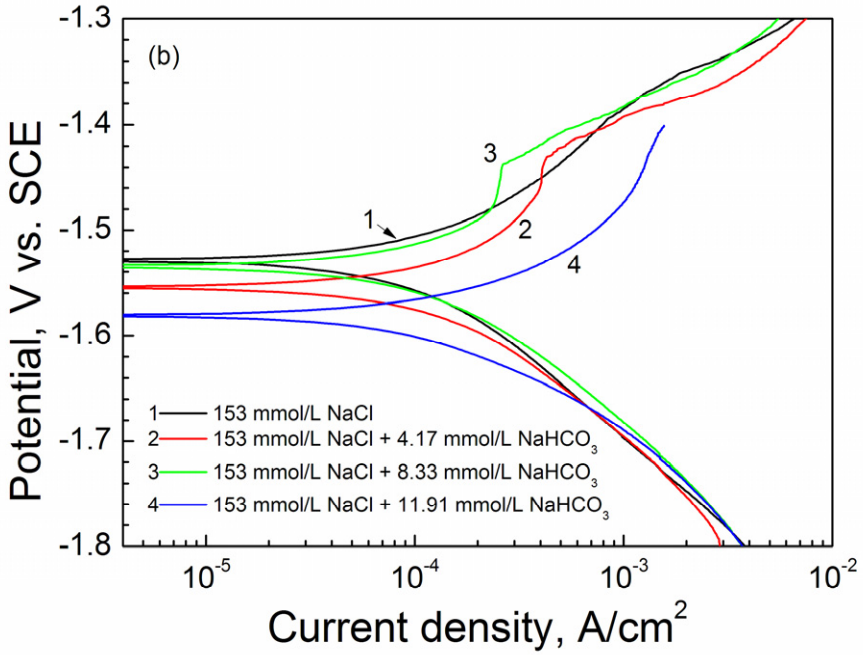

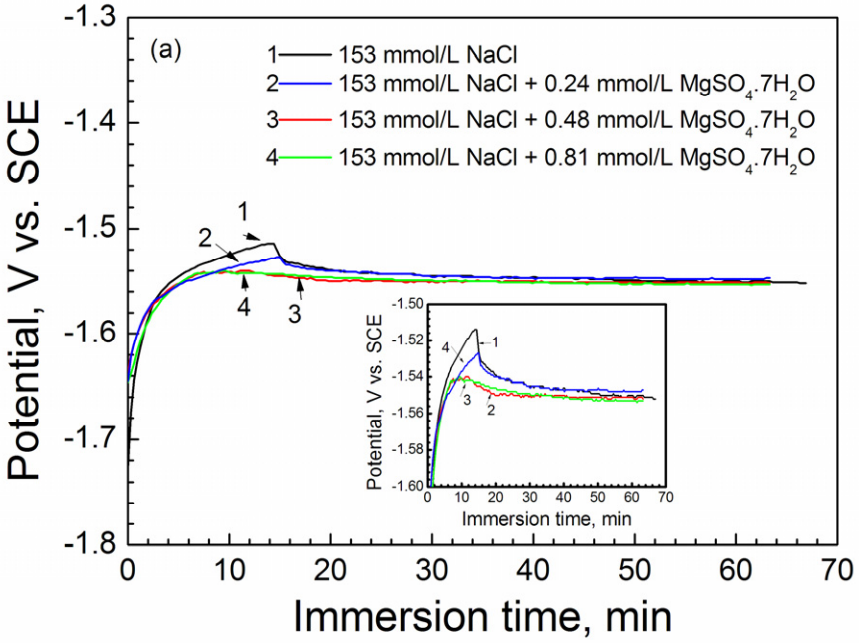

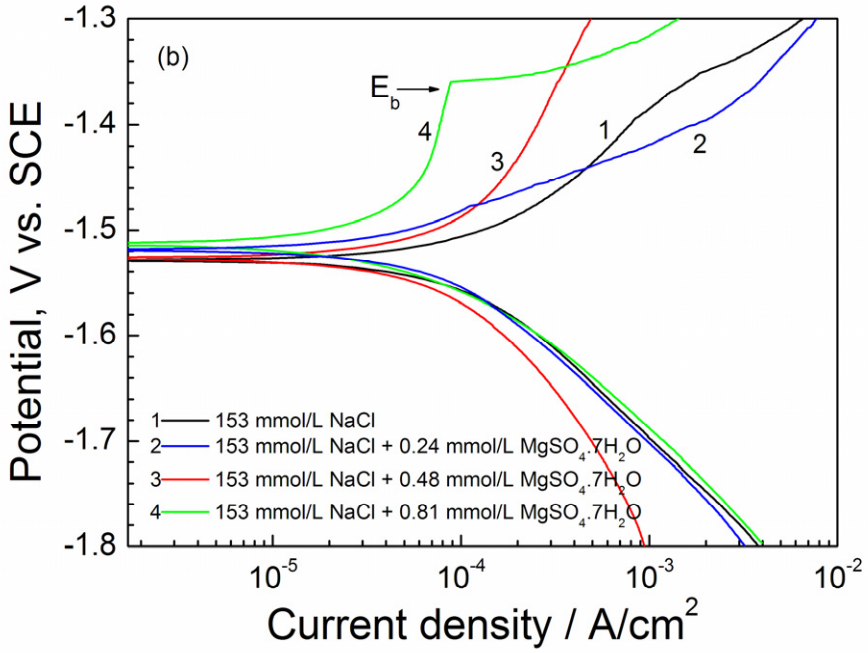

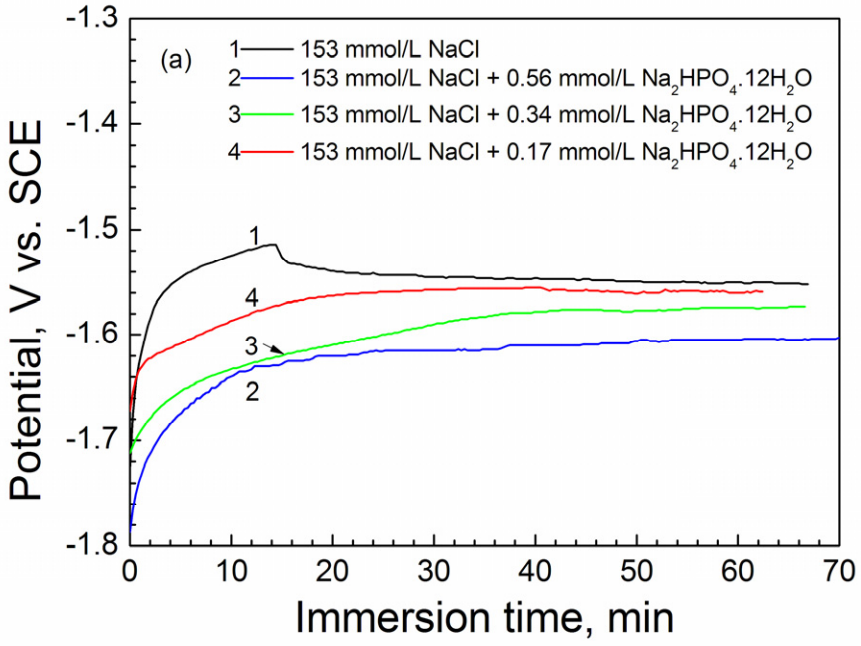

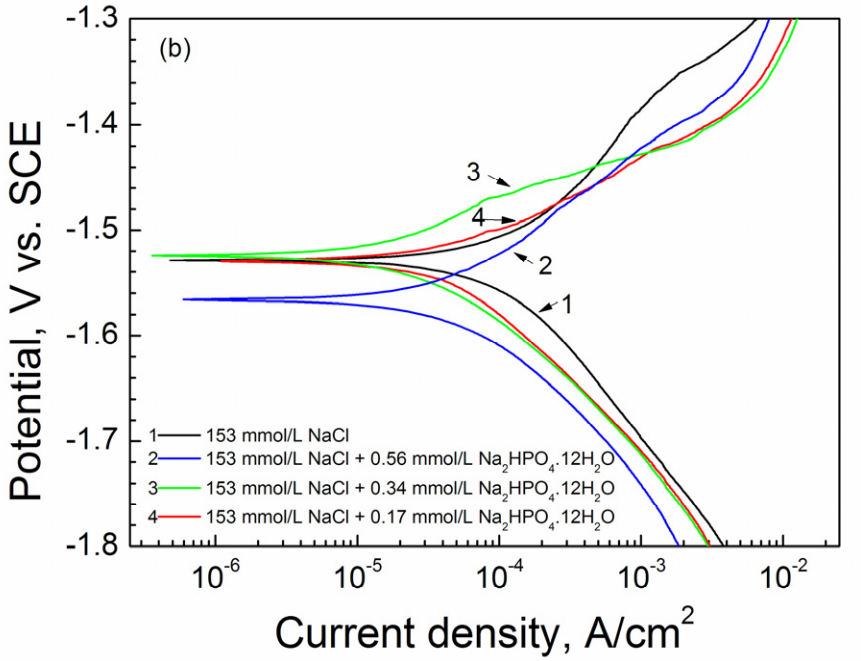

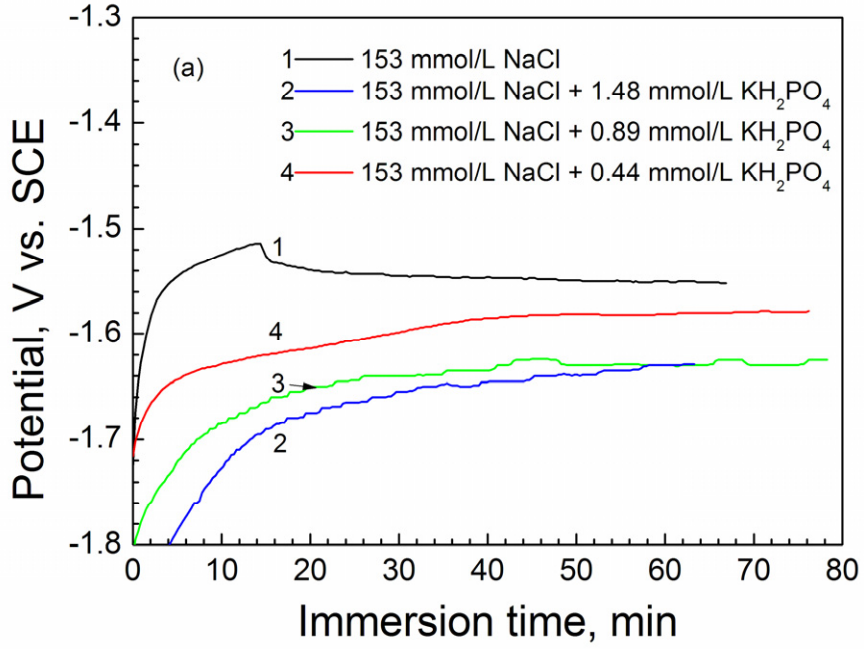

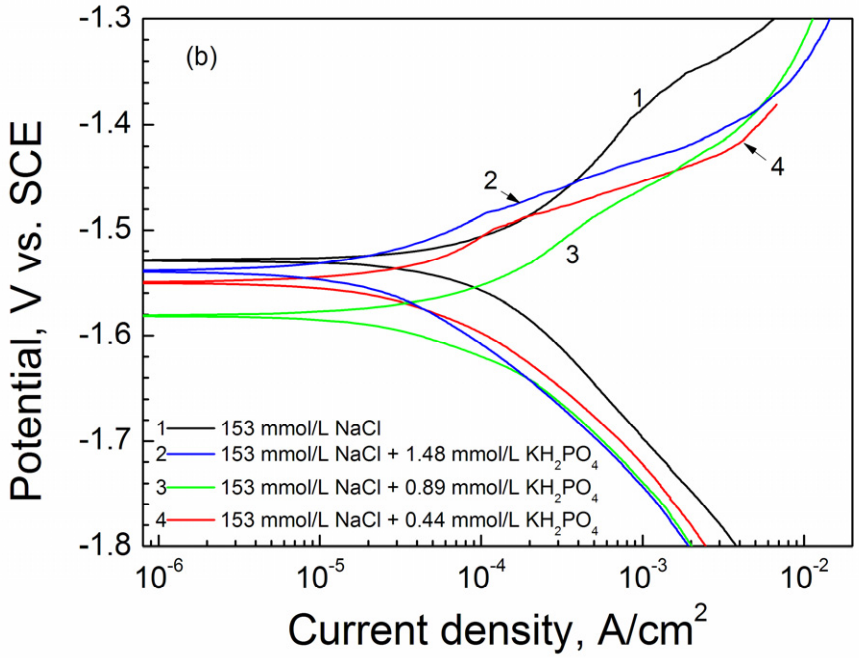

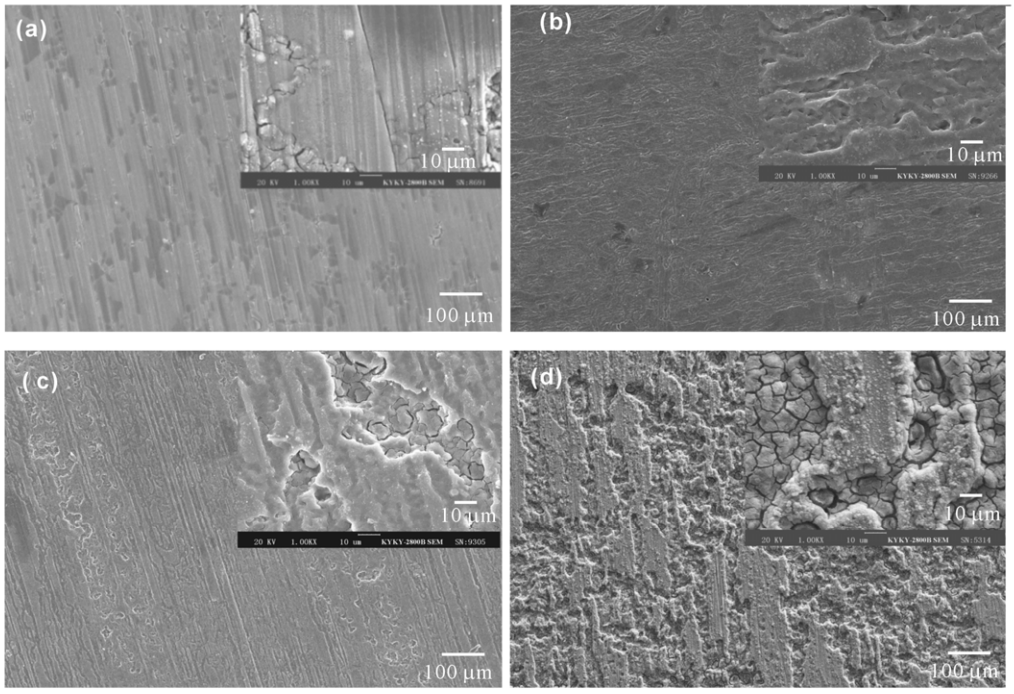

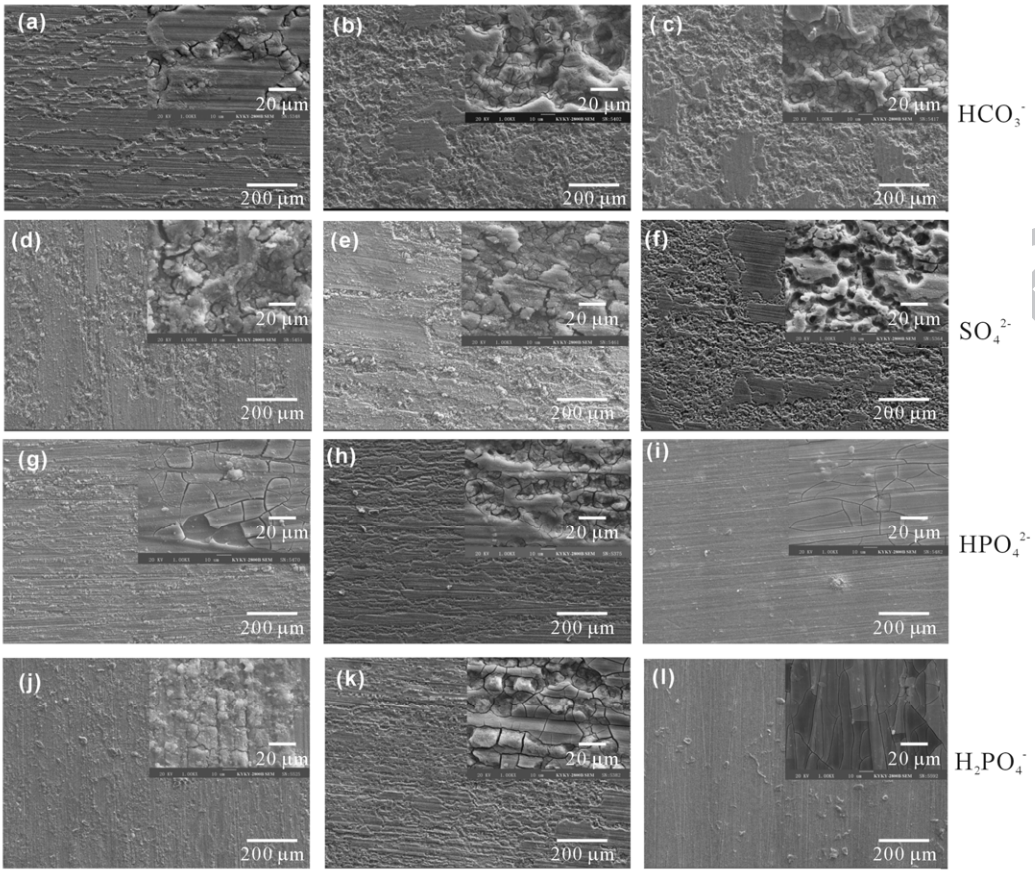

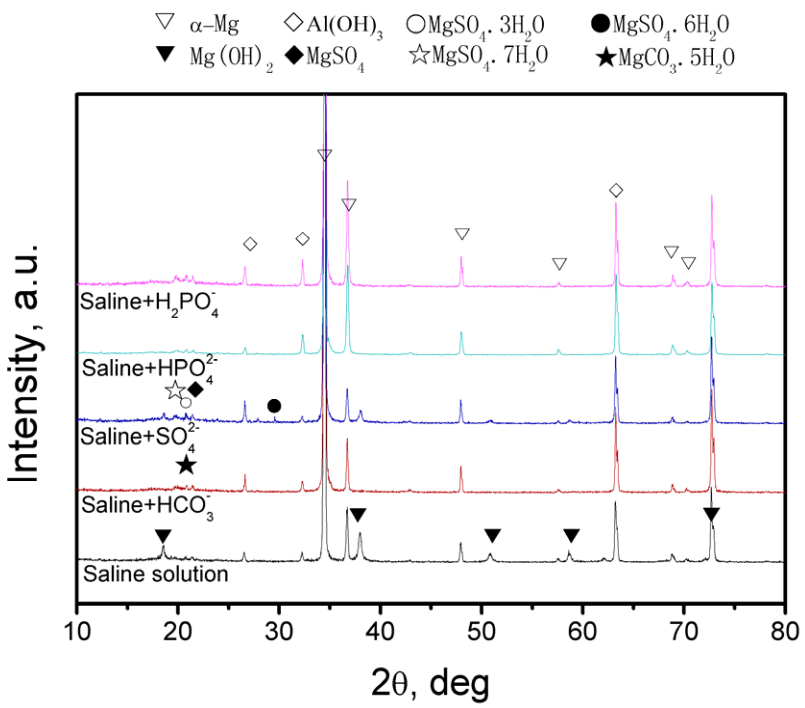

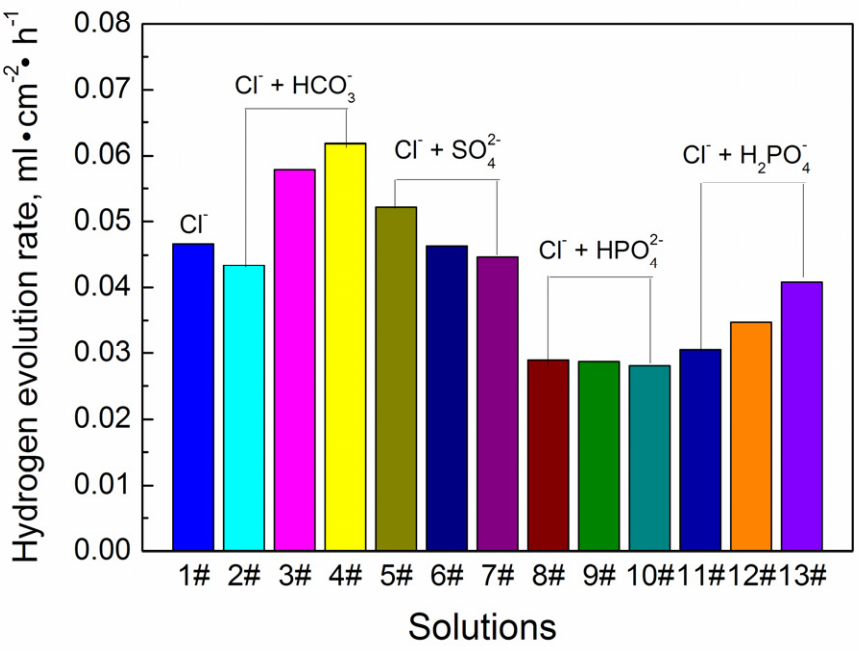

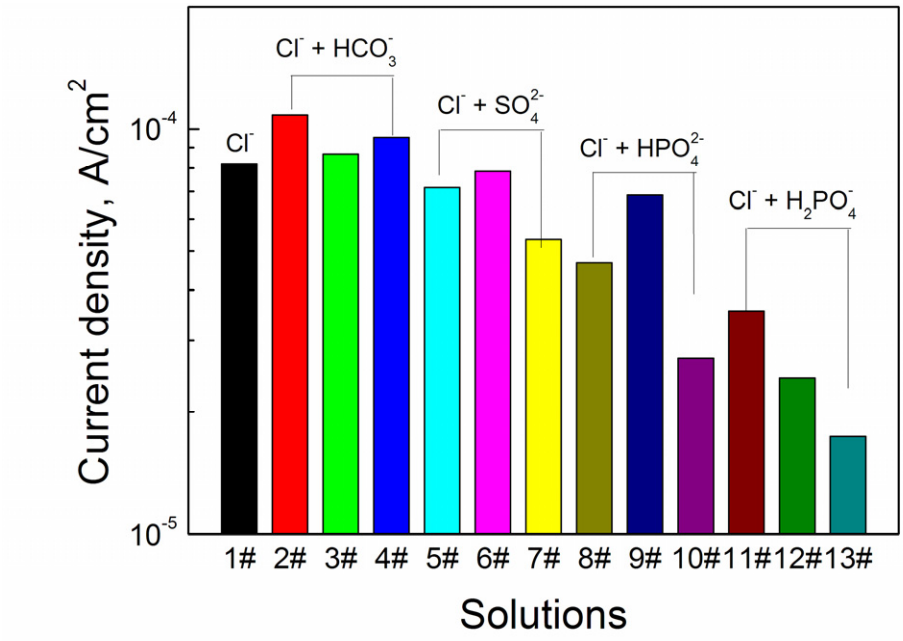

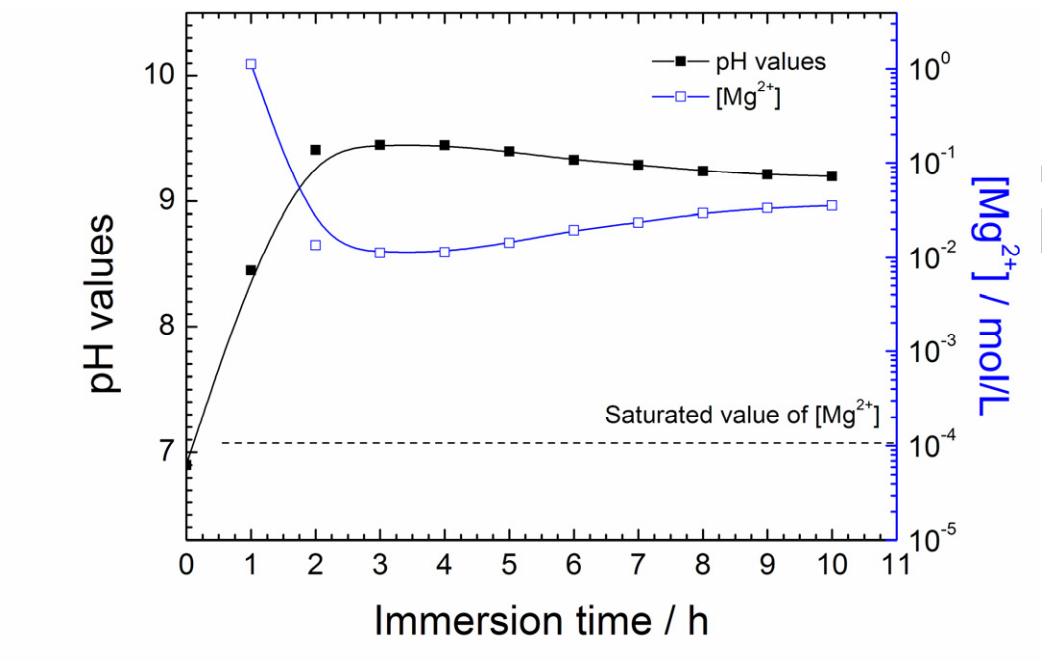

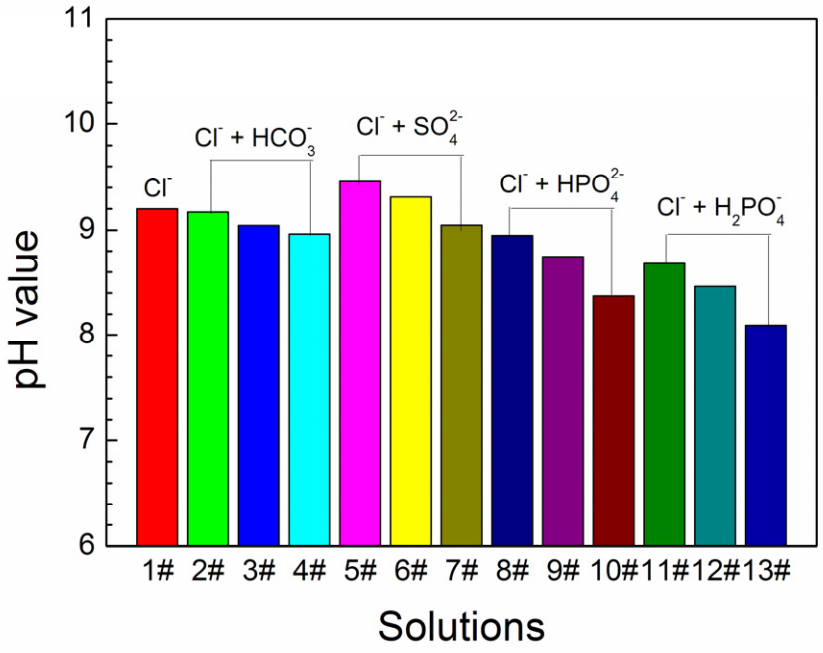

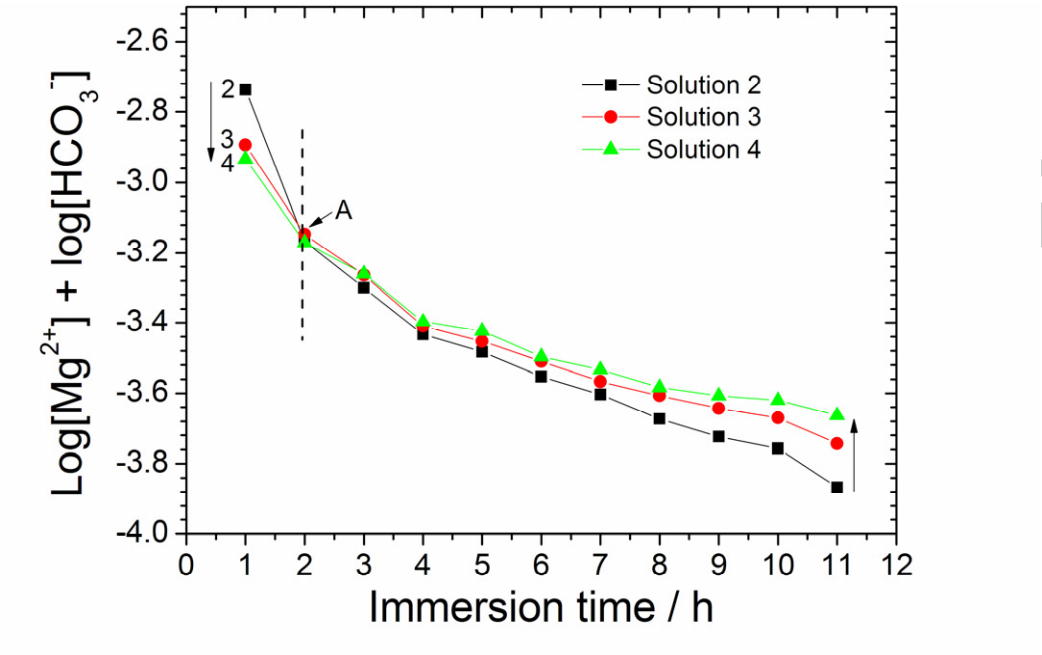

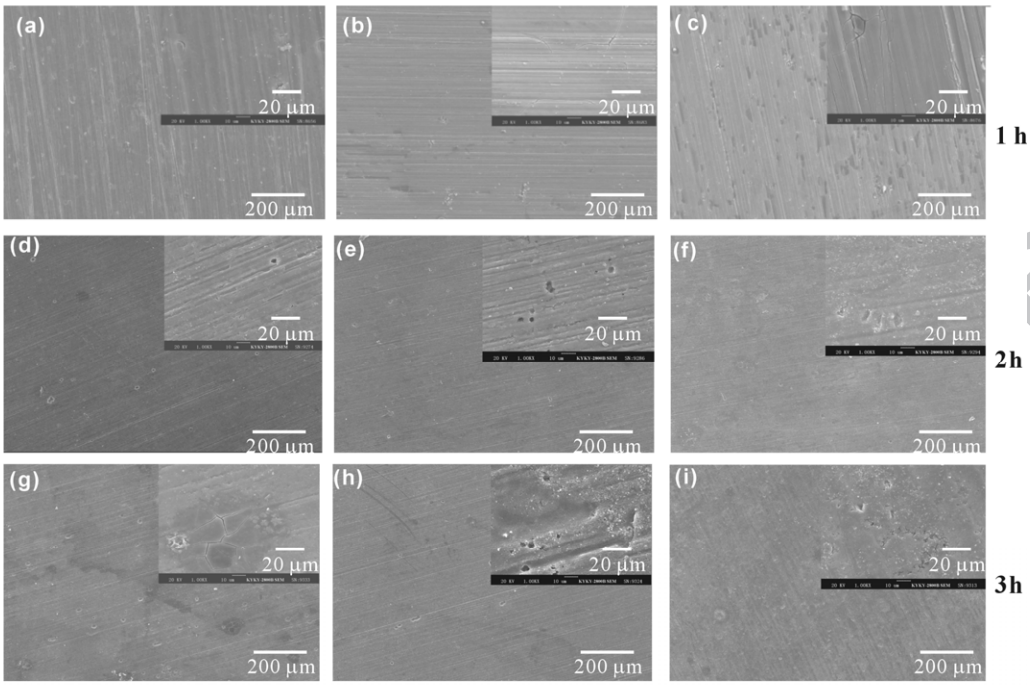

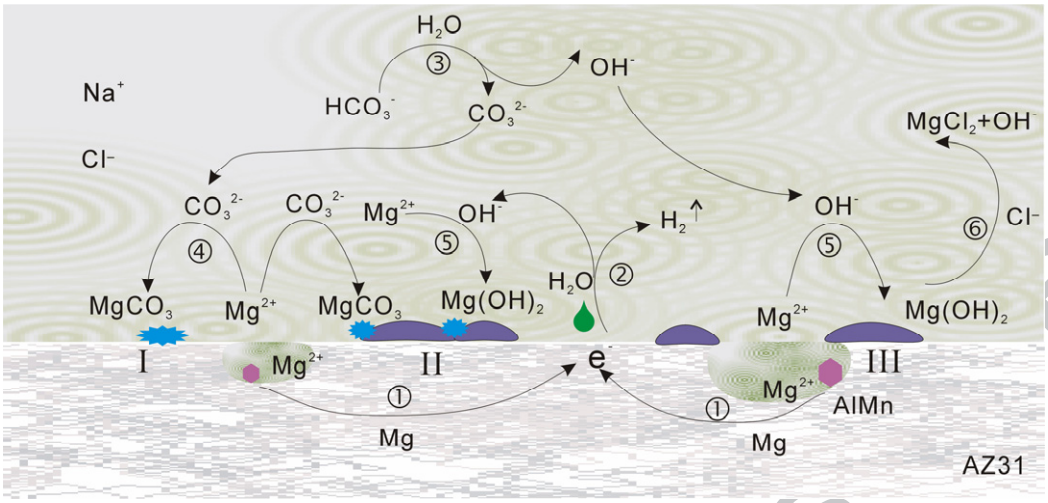

Tables

Table 1

Solutions	NaCl	$NaHCO_3$	$MgSO_4 \cdot 7H_2O$	$Na_2HPO_4 \cdot 12H_2O$	KH_2PO_4
1#	153.0				
2#	153.0	4.17			
3#	153.0	8.33			
4#	153.0	11.91			
5#	153.0		0.24		
6#	153.0		0.48		
7#	153.0		0.81		
8#	153.0			0.17	
9#	153.0			0.34	
10#	153.0			0.56	
11#	153.0				0.44
12#	153.0				0.89
13#	153.0				1.48

Table 2

Compounds	Formula	K_{sp}^{0}	Solubility, mol/L
Magnesium hydroxide	$Mg(OH)_2$	5.61×10^{-12}	1.1×10^{-4}
Magnesium carbonate	$MgCO_3$	6.82×10^{-8}	2.6×10^{-4}
Magnesium carbonate trihydrate	$MgCO_3\cdot3H_2O$	2.38×10^{-8}	
Magnesium carbonate pentahydrate	$MgCO_3\cdot5H_2O$	3.78×10^{-8}	
Magnesium phosphate	$Mg_3(PO_4)_2$	1.0×10^{-25}	5.4×10^{-7}

Graphical abstract

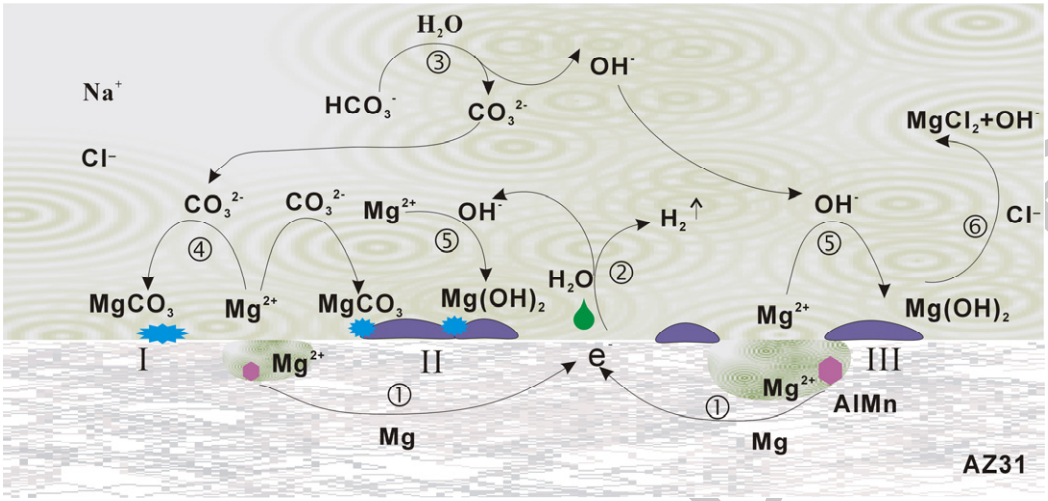

Highlights

► The presence of anions led to the formation of a corrosion product film. ► The presence of anions decreased open circuit potentials and changed corrosion rates. ► A model for the formation mechanism of magnesium carbonate film is proposed. ►The pH change with time cannot reflect the corrosion rates of Mg alloys.